AGU PUBLICATIONS

Geophysical Research Letters

RESEARCH LETTER
10.1002/2016GL070258

Key Points:
- In situ measure of abrasion beneath the Greenland Ice Sheet at 0.72 ± 0.35 mm yr-1
- Subglacial erosion rates in SW Greenland are significantly higher than typical erosion rates in Polar Regions
- Subglacial erosion in the Baffin Bay-Greenland region is linked to regional climate regimes

Supporting Information:
- Supporting Information S1
- Table S3

Correspondence to:
N. E. Young,
nicolasy@ldeo.columbia.edu

Citation:
Young, N. E., J. P. Briner, J. Maurer, and J. M. Schaefer (2016), ^{10}Be measurements in bedrock constrain erosion beneath the Greenland Ice Sheet margin, *Geophys. Res. Lett.*, *43*, 11,708–11,719, doi:10.1002/2016GL070258.

Received 30 JUN 2016
Accepted 2 NOV 2016
Accepted article online 4 NOV 2016
Published online 26 NOV 2016

©2016. American Geophysical Union. All Rights Reserved.

^{10}Be measurements in bedrock constrain erosion beneath the Greenland Ice Sheet margin

Nicolás E. Young[1], Jason P. Briner[2], Josh Maurer[3], and Joerg M. Schaefer[1,3]

[1]Lamont-Doherty Earth Observatory, Columbia University, Palisades, New York, USA, [2]Department of Geology, University at Buffalo, Buffalo, New York, USA, [3]Department of Earth and Environmental Sciences, Columbia University, New York, New York, USA

Abstract Glacial erosion is a key process driving landscape evolution, but it remains unclear what factors dictate the rate at which subglacial erosion occurs. Moreover, estimates of subglacial erosion that do not rely on sediment flux techniques are rare. Here, we present in situ ^{10}Be measurements from bedrock surfaces in western Greenland with well-constrained ice-cover histories to quantify the erosion rate beneath the Greenland Ice Sheet margin during historical times. We calculate an abrasion rate of 0.72 ± 0.35 mm yr^{-1} and a likely total basin-wide erosion rate (abrasion + quarrying) of ~1–1.8 mm yr^{-1}, which are at least 1 order of magnitude higher than typical subglacial erosion rates in other polar landscapes. A compilation of published ^{10}Be data suggests that the southwestern Greenland Ice Sheet acts as a particularly effective erosional agent within the broader Baffin Bay-Greenland region over millennial to glacial-interglacial timescales, suggestive of a basal ice sheet thermal regime controlled by regional climate.

1. Introduction

Warm-based glaciers erode their underlying terrain, but it remains difficult to quantify the rate at which ice modifies the landscape. The challenge in constraining subglacial erosion rates arises primarily from the simple fact that erosion occurs in a largely inaccessible environment that is buried by ice, and this lack of empirical measurements limits our ability to pinpoint glacier erosion's controlling mechanisms and hampers assessment of glacial erosion's efficacy in landscape modification [*Hallet et al.*, 1996; *Koppes and Montgomery*, 2009]. Whereas few studies have directly measured erosion beneath modern glaciers through repeat observations at isolated points [e.g., *Boulton*, 1979; *Cohen et al.*, 2005], methods of indirectly quantifying subglacial erosion that do not require access to the ice-bed interface are more often used. These alternative methods include theoretical calculations [*Harbor et al.*, 1988; *Ugelvig et al.*, 2016], laboratory experiments [*Iverson and Zoet*, 2015], sediment volume measurements in proglacial sediment depocenters and rivers [*Koppes et al.*, 2010, 2015; *Cowton et al.*, 2012; *Herman et al.*, 2015], and cosmogenic nuclide-based measurements in formerly glaciated landscapes [*Briner and Swanson*, 1998; *Stroeven et al.*, 2002; *Duhnforth et al.*, 2010; *Goehring et al.*, 2011]. These approaches, however, typically only provide point estimates or yield an integrated basin-wide view of erosion and are unable to capture the potential spatial variability in subglacial erosion beneath glaciers. Moreover, erosion rates derived from sediment-based studies are susceptible to sediment transfer biases, potentially resulting in artificially high erosion rates, and assumptions in the glacial and erosional history of targeted landforms in cosmogenic nuclide-based studies can prevent firm erosion rate estimates. Many estimates of subglacial erosion are also linked to glaciers that are currently retreating where increased meltwater discharge and dynamical processes can result in temporally brief enhanced erosion rates [*Jaeger and Koppes*, 2016]. Indeed, modern subglacial erosion rates inferred from sediment-based methods are an order of magnitude greater than glacial-interglacial scale erosion rates and up to 2 orders of magnitude greater than erosion rates measured over the Quaternary [*Koppes and Montgomery*, 2009].

Not only does it remain difficult to quantify the magnitude and rate of erosion beneath glaciers but also there are very few empirical measurements of subglacial erosion beneath ice sheets. Better measurements of glacier erosion beneath ice sheets can offer key insights into the processes influencing basal slip and ice motion —processes that impact ice sheet stability and behavior. Several geophysical ice sheet models employ a shallow-ice approximation where friction between basal ice and the underlying substrate is the only stress that opposes ice motion, and furthermore, basal sliding is a key parameter that affects modeled ice sheet behavior [*Greve et al.*, 2011; *Applegate et al.*, 2012; *Lecavalier et al.*, 2014]. Here we use in situ cosmogenic ^{10}Be measurements from morphostratigraphically distinct bedrock surfaces adjacent to Sermeq Kujalleq

(Jakobshavn Isbræ) to quantify subglacial erosion rates and their spatial pattern beneath the Greenland Ice Sheet margin (GrIS; Figure 1). We place these constraints in a broader framework by assembling a large database of ^{10}Be ages from the Baffin Bay-Greenland region to identify the dominating factors controlling subglacial erosion.

1.1. The Sermeq Kujalleq Region

Sermeq Kujalleq, western Greenland, drains ~7% of the GrIS and is the ice sheet's fastest outlet glacier reaching seasonal speeds of up to ~17 km yr^{-1} [*Rignot and Kanagaratnam*, 2006; *Joughin et al*., 2014]. In contrast to the marine-terminating Sermeq Kujalleq, ice velocities of only a few tens of m yr^{-1} characterize the adjacent land-terminating margin [*Joughin et al*., 2010]. This disparity in marine- versus land-terminating ice-margin dynamics is also consistent with the geologic record of ice-margin change; since ~1850 C.E. (Common Era) Sermeq Kujkalleq has retreated ~35 km up fjord, but the adjacent land-terminating margins have retreated ~2–4 km [*Weidick and Bennike*, 2007; *Csatho et al*., 2008]. Retreat of the land-terminating margin has uncovered a landscape characterized by sculpted and striated crystalline bedrock (gneiss) [*Garde and Steenfelt*, 1999] positioned between the ~1850 C.E. ice limit, referred to as the "historical moraine," and the current ice margin located to the east (Figure 1). This freshly exposed bedrock presents an ideal opportunity to quantify the magnitude and rate of erosion that occurs beneath the GrIS margin. We sampled eight bedrock locations immediately inboard (~190–550 m) of the historical moraine for in situ cosmogenic ^{10}Be measurements and compare these measurements with detailed geological and historical records of ice-margin change through the Holocene (Figure 1).

1.2. Ice-Margin History Through the Holocene

In order to constrain the magnitude and rate of subglacial erosion at our bedrock locations, the Sermeq Kujalleq forefield's complete subaerial exposure and ice-cover history must be known. Published ^{10}Be ages from bedrock surfaces located immediately outboard (west) of the historical moraine all statistically overlap and indicate that deglaciation occurred 7520 $\pm$ 170 years ago (n = 8; 1 outlier removed; $\pm$ SD) (Figure 1) [*Young et al*., 2011]. These outboard ^{10}Be ages span tens of kilometers, and yet their ^{10}Be ages are statistically identical and show no trend in age with distance from the ice margin indicating that local deglaciation occurred rapidly at ~7.5 ka. In addition, these outboard ^{10}Be ages include samples that were collected within tens of meters of the historical moraine and only ~550 m west of our targeted bedrock locations inboard of the historical moraine. Because of the close proximity between the outboard ^{10}Be ages with our inboard bedrock locations, the deglaciation age of 7520 $\pm$ 170 years ago also marks the timing of initial deglaciation and start of the cosmogenic clock for the landscape located immediately inboard of the historical moraine.

Lake sediment records from proglacial-threshold lakes, combined with historical observations in the Sermeq Kujalleq region, constrain the timing of when the landscape located immediately inboard of the historical moraine became ice covered as the GrIS advanced and approached the historical limit [*Briner et al*., 2010]. When the GrIS terminus is within a threshold lake's drainage catchment (but not overriding the lake), the lake receives silt-laden GrIS meltwater. When the GrIS terminus is not in the lake's catchment, meltwater inflow ceases and the lake is dominated by organic sedimentation; these two modes of sedimentation result in a distinct "on-off" sedimentary signature. At Iceboom Lake (informal name; Figure 2), maximum-limiting radiocarbon ages at the contact between the upper minerogenic unit and the underlying organic unit reveal that the GrIS margin approached its historical maximum ~400 cal yr B.P. Moreover, this was the only time over the last ~7.5 ka that the GrIS approached its eventual historical maximum limit as indicated by the continuous organic sedimentation that occurred since basin deglaciation until deposition of the minerogenic unit dated to ~400 cal yr B.P. [*Young et al*., 2011]. Further analysis of Iceboom Lake's sediments reveals that this uppermost minerogenic unit is varved (annually laminated), and annual layer counting of this minerogenic unit suggests that GrIS meltwater began entering the lake's drainage basin at 1820 $\pm$ 5 C.E. as the GrIS advanced toward its historical maximum position [*Briner et al*., 2011]. Whereas the maximum-limiting radiocarbon ages indicate that the GrIS approached its historical maximum ~400 cal yr B.P., the varved sediments indicate that the GrIS did not approach its historical maximum until 1820 $\pm$ 5 C.E. Considering the relatively low sedimentation rate of this site (~68 cm deposition in ~7.5 ka), the offset between the radiocarbon-based age of the contact and the varve-based age is not necessarily unexpected because, again, the radiocarbon age only provides a maximum-limiting age. To better assess whether the GrIS began to approach its historical maximum at ~400 cal yr B.P. or at 1820 $\pm$ 5 C.E., we look to a similar and independent sediment record from a nearby basin.

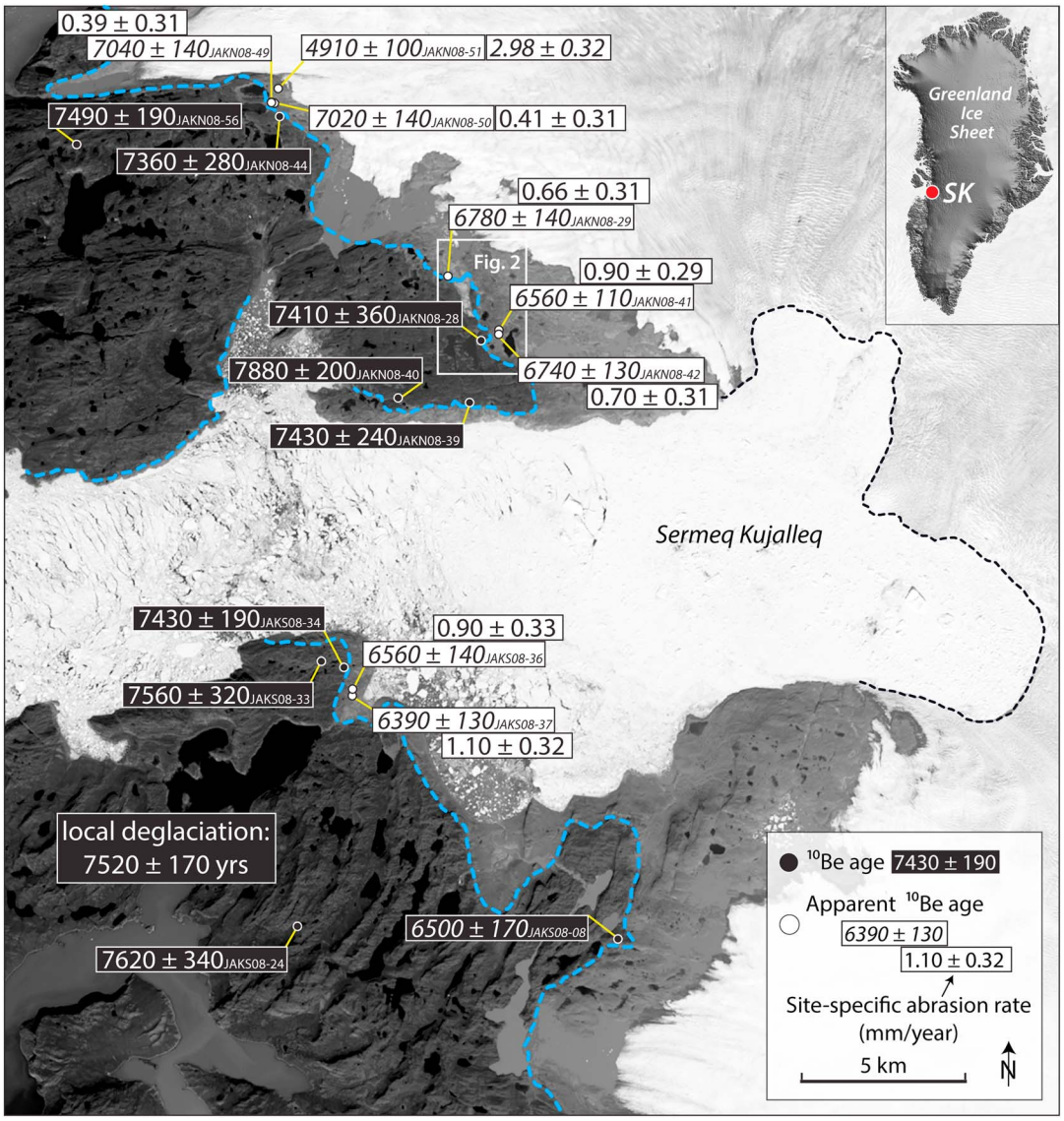

Figure 1. The Sermeq Kujalleq (SK) forefield with the historical moraine and trimline outlined in light blue. Shown are ^{10}Be ages from outboard of the historical maximum (black boxes; white text) that all statistically overlap and constrain local deglaciation to 7520 ± 170 years ago. All ^{10}Be ages have been recalculated using the Baffin Bay production rate and Lm scaling [*Young et al.*, 2013a]. Apparent ^{10}Be ages from immediately inboard of the historical moraine (white boxes, black text) are shown with the site-specific abrasion rate. Base image is a Landsat 8 image collected on 29 July 2015.

Immediately northeast of Iceboom Lake, Glacial Lake Morten (informal name; now drained) contains laminated lake sediments draped over a preserved vegetated landscape marking the transition from a tundra landscape to a proglacial lake basin as the GrIS advanced to dam the valley. Maximum-limiting radiocarbon ages ($n = 3$) from the paleotundra surface marking the transition to a proglacial lake return a calibrated summed probability with prominent solutions at ~1650–1690 C.E., 1730–1810 C.E., and modern times (Figure 2). Similar to at Iceboom Lake, layer counting of Glacial Lake Morten's varved sediments reveals that the valley was dammed by the advancing GrIS at ~1795–1800 C.E., consistent with the Glacial Lake Morten basal radiocarbon solution of 1730–1810 C.E. and consistent with the estimate of 1820 ± 5 C.E. from Iceboom Lake (Figure 2) [*Briner et al.*, 2011].

Sediments from both Iceboom Lake and Glacial Lake Morten indicate that the GrIS approached its historical maximum ~ 1800 C.E., but a closer look at each lake's morphostratigraphic position allows us to fine tune the GrIS's advance history during the late Holocene. Glacial Lake Morten rests closer to the GrIS margin and is

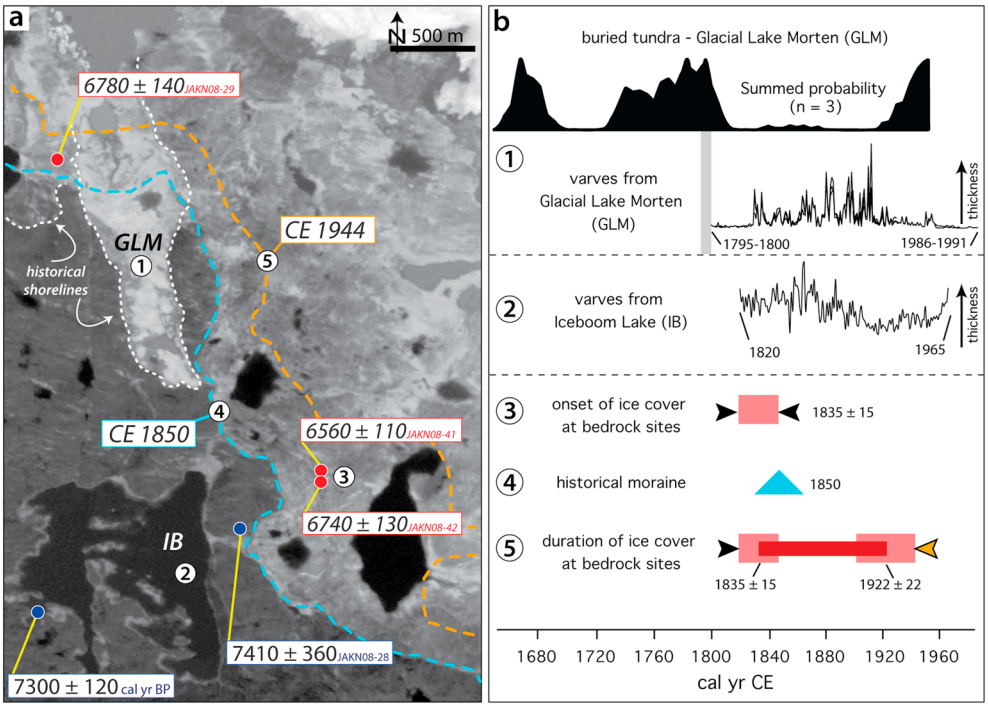

Figure 2. (a) Map showing the detailed ice-margin history of the western GrIS during historical times. (b) Timeline of the GrIS advance and retreat cycle during historical times; numbers are linked to Figure 2a. (1) As the GrIS advances from the east, Glacial Lake Morten (GLM) becomes a proglacial lake first. Shown is the calibrated summed probability of ^{14}C ages ($n = 3$) from a tundra surface buried by varved glacial lake sediments. Also shown is the number of varves dating back to 1795–1800 C.E. in GLM [*Briner et al.*, 2011]. (2) Varves from Iceboom Lake indicate that the lake became a proglacial lake at ~ 1820 C.E. (3) Bedrock sites must become covered by the advancing GrIS after ~ 1820 C.E. but before 1850 C.E. when historical observations indicate that the GrIS had already reached its historical moraine [*Weidick*, 1968]. (4) Deposition of the historical moraine by 1850 C.E. (5) Aerial imagery reveals that our bedrock sites had become ice free before 1944 C.E. [*Csatho et al.*, 2008]. Figure 2a is a SPOT image collected in 2007.

positioned east of Iceboom Lake, and thus, as the GrIS margin advanced, Glacial Lake Morten became a proglacial lake before Iceboom Lake (Figure 2). In addition, the topographic threshold that the GrIS margin crossed in order for Iceboom Lake to receive GrIS meltwater and become a proglacial lake is positioned east of our targeted bedrock locations and the historical moraine. Therefore, Iceboom Lake began receiving GrIS meltwater prior to (1) the GrIS covering our bedrock locations and (2) the GrIS achieving its maximum historical limit situated near the eastern shoreline of the lake. Historical observations confirm that the GrIS reached its historical maximum before 1850 C.E. [*Weidick*, 1968], and Iceboom Lake sediments indicate that the GrIS reached the historical limit sometime after 1820 ± 5 C.E. Therefore, the landscape just inside the historical moraine became ice covered at 1835 ± 15 C.E. (midpoint between 1820 and 1850 C.E.). We cannot pinpoint the exact timing of when the GrIS retreated back to the east and reexposed the bedrock surfaces located just inboard of the historical moraine, but historical observations indicate that the ice margin remained near the historical moraine until at least 1900 C.E. [*Weidick*, 1968], and aerial imagery reveals that the ice margin was situated just east of our sample locations in 1944 C.E. [*Csatho et al.*, 2008]. Conservatively, the bedrock surfaces became ice free at 1922 ± 22 C.E. (midpoint between 1900 and 1944 C.E.).

In summary, following early Holocene deglaciation 7520 ± 170 years ago, our targeted bedrock sites became reoccupied by ice at 1835 ± 15 C.E., before being reexposed at 1922 ± 22 C.E. as the GrIS retreated from its historical moraine. Combined, geological and historical records of ice-margin change indicate that only 87 ± 27 years ($\sqrt{(15^2 + 22^2)}$) of historical ice cover separates the bedrock surfaces located immediately inboard and outboard of the historical moraine (see supporting information). It is possible that all of our sites did not experience the same duration of historical ice cover, but the relatively consistent location of our sites with respect to the historical moraine makes it unlikely that there were large site-to-site differences in ice-cover duration across our field area. Thus, considering the almost identical subaerial exposure histories of

the two bedrock surfaces, ^{10}Be ages from inboard of the historical moraine should be similar to the existing ^{10}Be ages from bedrock located outside the historical moraine if no subglacial erosion has occurred; younger inboard ^{10}Be ages reflect erosion beneath the GrIS during 87 ± 27 years of historical ice cover.

2. Methods and ^{10}Be Measurements

We sampled eight abraded bedrock surfaces for ^{10}Be analysis (Figures 1 and 2), and because we focused exclusively on abraded surfaces, our ^{10}Be measurements most likely only quantify subglacial abrasion. All samples were processed at the Lamont-Doherty Earth Observatory Cosmogenic Laboratory following standard Be extraction methods [*Schaefer et al.*, 2009], and final ^{10}Be/^{9}Be ratios were measured at the Lawrence Livermore National Laboratory—Center for Accelerator Mass Spectrometry relative to the 07KNSTD standard (Table S1) [*Nishiizumi et al.*, 2007]. We present and discuss ^{10}Be measurements as ^{10}Be ages calculated using modified CRONUS calculator code and the regionally calibrated Baffin Bay ^{10}Be production rate with "Lm" scaling [*Balco et al.*, 2008; *Young et al.*, 2013a; *Lal*, 1991; *Stone*, 2000], but note that our results are insensitive to the choice of production rate or scaling scheme because we base our discussion on the difference in ^{10}Be concentration between inboard and outboard samples. And we do not consider the ^{10}Be production rate uncertainty in our discussion because we are only comparing ^{10}Be ages to each other and are not comparing ^{10}Be ages to any independent time series.

3. ^{10}Be Ages and Erosion

Our new ^{10}Be ages from bedrock located inboard of the historical moraine range from 4900 ± 100 to 7040 ± 140 years (n = 8; 1σ analytical uncertainties of 1.7–2.2%; Table S1). To quantify the total and rate of erosion during the period of historical ice cover at our bedrock sites (87 ± 27 years), we compare these measured ^{10}Be concentrations (ages) to modeled site-specific ^{10}Be production-depth profiles in bedrock (Figure 3). If no erosion has occurred, then measured bedrock ^{10}Be concentrations should equate to the timing of deglaciation (7520 ± 170 years) minus the duration of ice cover (87 ± 27 years). Our apparent ^{10}Be ages ranging from 4900 ± 100 to 7040 ± 140 years are significantly less than this value (7433 ± 173 years; uncertainty in ice-cover duration is propagated quadratically) and allow us to quantify subglacial erosion through the modeled ^{10}Be production-depth profile in bedrock toward lower ^{10}Be concentrations (i.e., younger apparent ^{10}Be ages). Using this approach, total erosional depths range from 3.35 ± 2.68 cm to 25.94 ± 2.79 cm (Figure 3 and Table S2; see supporting information), and assuming 87 years of ice cover, site-specific abrasion rates range from 0.39 ± 0.31 mm yr^{-1} to 2.98 ± 0.32 mm yr^{-1} (Figures 1 and 3 and Table S2). With the exception of one sample north of Sermeq Kujalleq (JAKN08-51; 2.98 ± 0.32 mm yr^{-1}) all of the site-specific abrasion rates are ≤1 mm yr^{-1} and average 0.72 ± 0.26 mm yr^{-1} (n = 7). It is possible that the value of 2.98 ± 0.32 mm yr^{-1} truly reflects that site's amount of abrasion; however, adjacent abrasion rates of 0.39 ± 0.31 mm yr^{-1} and 0.41 ± 0.30 mm yr^{-1} are significantly lower and consistent with all remaining abrasion rates. The value of 2.98 ± 0.32 mm yr^{-1} is likely an outlier, perhaps influenced by Holocene sediment cover or subglacial quarrying (see supporting information). Finally, after propagating through the uncertainty in the duration of ice cover at our sample locations (27 years), we calculate an average abrasion rate of 0.72 ± 0.35 mm yr^{-1} in the Sermeq Kujalleq forefield. We also acknowledge that our ice-margin chronology theoretically allows for end-member ice-cover durations as short as 50 years (1850–1900 C.E.) and as long as 147 years (1820–1944 C.E.), but these durations would require what are extreme and unlikely rates of ice advance and retreat (see supporting information). Nonetheless, using these end-member ice-cover durations would result in erosion rates that increase by 79% and decrease by 29%, respectively. Finally, our abrasion rate of 0.72 ± 0.35 mm yr^{-1} is not a measure of total basin-wide erosion because it does not account for glacial quarrying. Although we were unable to quantify glacial quarrying, previous work suggests that ~30–60% of the total basin-wide subglacial erosion budget is attributable to glacial quarrying [*Gurnell*, 1987; *Hallet et al.*, 1996; *Riihimaki et al.*, 2005], and thus, we estimate that total basin-wide erosion in this region occurs at ~1–1.8 mm yr^{-1}.

4. Differential Subglacial Erosion Beneath the GrIS and Climate

Site-specific abrasion rates are remarkably consistent suggesting that abrasion across the Sermeq Kujalleq forefield occurs in a relatively uniform fashion. Although abrasion can be governed by the effective normal pressure at the bed and ice sliding velocity, which can vary from location to location, our consistent abrasion

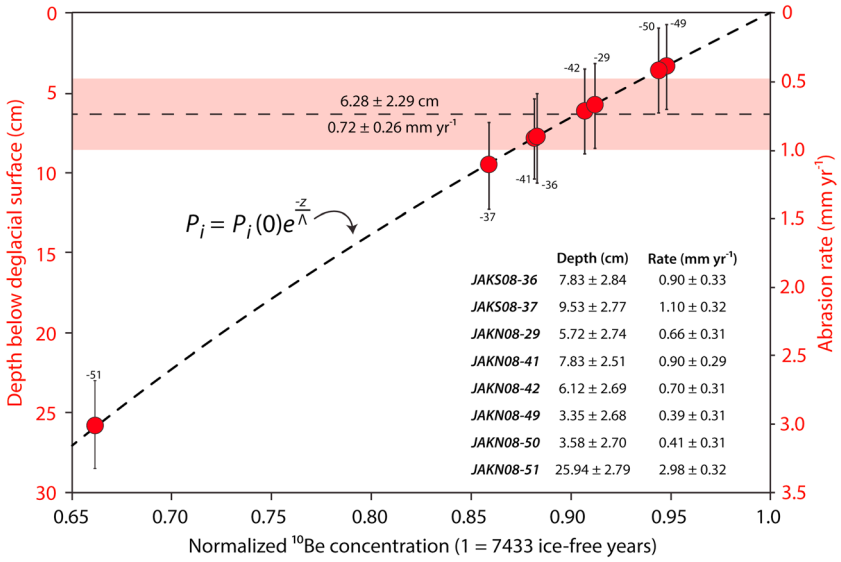

Figure 3. Total modeled ^{10}Be production with depth in bedrock (dashed line). A normalized ^{10}Be concentration of 1 equals the timing of regional deglaciation minus the duration of historical ice cover (7433 ± 173 years); the uncertainty in this value is reflected in the individual measurement error bars. Production by spallation and muons is calculated independently, and the ^{10}Be production with depth (dashed line) is the summation of production by spallation and muons, muons according to *Heisinger et al.* [2002a, 2002b]. Z is the mass depth below the surface expressed in g cm^{-2} and is the product of depth (cm) and material density (g cm^{-3}). P_i is the production rate of ^{10}Be (atoms g^{-1} yr^{-1}) by spallation or muons at depth z. P_i (0) is the surface production rate via spallation or muons. Λ is the effective attenuation length (spallation = 160 g cm^{-2}, slow muons = 1510 g cm^{-2}, and fast muons = 4300 g cm^{-2}). We use a typical rock density of 2.65 g cm^{-3} for gneiss. Red symbols mark the depths below the deglacial surface along the ^{10}Be production-depth profile that the measured ^{10}Be concentrations equates to and their corresponding abrasion rates. Note that the ^{10}Be production-depth profile is not fit to the data points and that any ^{10}Be measurement will fall somewhere along the depth profile.

rates suggest that the GrIS thickness and sliding velocities across our sample sites were similar during the period of historical ice cover. We note that the lowest abrasion rates of 0.39 ± 0.31 mm yr^{-1} and of 0.41 ± 0.31 mm yr^{-1} occur at our most distal location from Sermeq Kujalleq, and abrasion rates appear to increase toward Sermeq Kujalleq (Figure 1). This pattern is consistent with increasing abrasion toward the main outlet glacier where ice velocities are significantly higher, but for now, this relationship remains tentative due to the limited size and resolution of our sample set.

There are few estimates that constrain erosion beneath the GrIS. In eastern Greenland, sediment packages fronting fjords suggest that subglacial erosion occurs at the rate of 0.01 to 0.04 mm yr^{-1} [*Andrews et al.*, 1994]. More recently, sediment flux data from a proglacial river emanating out of Leverett glacier in southwestern Greenland point to a much higher erosion rate of 4.6 ± 2.6 mm yr^{-1} (Figure 4) [*Cowton et al.*, 2012] and similar sediment flux data from the nearby Watson River put forth an erosion rate of 0.58 mm yr^{-1} [*Wimpenny et al.*, 2010]; this latter estimate is based on 1 year's measurements and considered tentative. The inferred erosion rate at the Leverett glacier is significantly higher than erosion near Sermeq Kujalleq, but to some degree this is to be expected. The Leverett glacier is a land-terminating outlet glacier where ice velocities are up to a few hundreds of m yr^{-1}, whereas ice velocities adjacent to Sermeq Kujalleq are only a few tens of m yr^{-1}, and the availability of meltwater at Leverett glacier may be contributing to increased erosion [*Cowton et al.*, 2012]. It is worth noting, however, that the calculated erosion rate at Leverett glacier is dependent on the area of the drainage catchment that the total sediment flux is averaged over. The Leverett glacier erosion rate decreases considerably, perhaps down to 1.0 ± 0.5 mm yr^{-1}, when accounting for a larger catchment area under the current GrIS [*Cowton et al.*, 2012].

Syntheses of global subglacial erosion rates reveal that erosion varies by orders of magnitude from ~0.01 mm yr^{-1} in polar settings up to ~100 mm yr^{-1} for temperate sites such as southeast Alaska [*Hallet et al.*, 1996; *Koppes and Montgomery*, 2009]. This wide range in erosion rates reflects different subglacial thermal regimes, ice sliding velocities, bedrock lithology, basin size, regional climate, tectonic activity, and

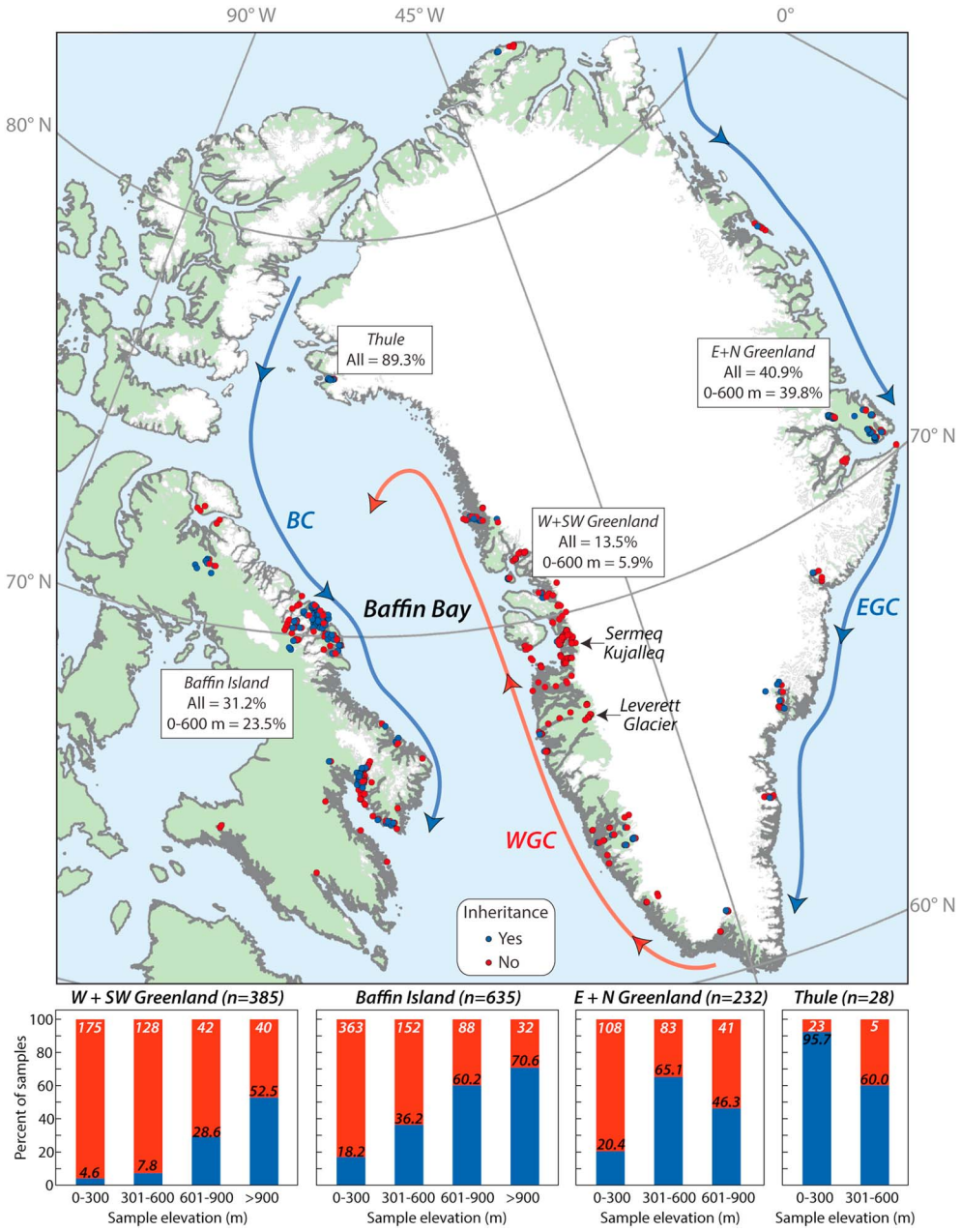

Figure 4. The Baffin Bay-Greenland region with published ^{10}Be ages ($n = 1280$). ^{10}Be ages marked with (blue dots) and without (red dots) isotopic inheritance follow the author's original interpretation (see supporting information for full reference list). Shown for each region is the total percentage of all measurements with inheritance and the percentage of samples between 0 and 600 m with inheritance. Histograms below show the total number of samples within each elevation band and the percentage of those samples with inheritance. BC: Baffin Current, EGC: East Greenland Current, WGC: West Greenland Current.

role of glacier dynamics. Perhaps most relevant here, however, are estimates of subglacial erosion from high latitudes that are generally under 0.1 mm yr^{-1} [*Hallet et al.*, 1996; *Koppes and Montgomery*, 2009; *Koppes et al.*, 2015]. Both the abrasion and overall erosion rate from the Sermeq Kujalleq region of 0.72 ± 0.35 mm yr^{-1} and ~1-1.8 mm yr^{-1}, respectively, and the erosion rate of 4.6 ± 2.6 mm yr^{-1} from the Leverett glacier, are significantly higher than the previously reported values from polar landscapes and the canonical Greenland subglacial erosion rate of ~0.01 mm yr^{-1} [*Hallet et al.*, 1996]. Thus, these results indicate that at least some sectors of the GrIS are capable of significant erosion approaching the efficacy of temperate mountain glaciers. On the

other hand, elevated erosion rates along southwestern Greenland stand out as anomalously high among subglacial erosion rates in Polar regions.

Recent work suggests that subglacial erosion is more strongly linked to regional climate and glacier thermal regime rather than ice flux or sliding speeds [*Koppes et al*., 2015]. Within this framework, elevated erosion along southwestern Greenland is to be expected. Southwestern Greenland's relatively mild climate is governed by the warm West Greenland Current making southwest Greenland the most temperate zone within the broader Baffin Bay region (Figure 4). By comparison, northern and eastern Greenland and Baffin Island are strongly influenced by Arctic Ocean water exiting through Fram and Nares straits, respectively. We suggest that the contrasting climates between southwestern Greenland versus the broader Baffin Bay region and eastern Greenland influence the overall glacier thermal regime, whereby ice at the ice sheet margin is primarily warm based in southwest Greenland and cold based to polythermal elsewhere; these differences are expressed in the glacial-geologic record.

Because there are only a limited number of subglacial erosion estimates around Greenland, an alternative proxy for subglacial erosion is needed to fully assess the spatial pattern of subglacial erosion and its relation to regional climate. In lieu of direct constraints of subglacial erosion, we compiled a database of published ^{10}Be ages from Greenland and Baffin Island to assess the magnitude of subglacial erosion beneath the GrIS and Laurentide Ice Sheet during the last glacial cycle ($n = 1280$; see supporting information and Appendix A below for full reference list). Approximately 3 m of subglacial erosion is needed to remove any ^{10}Be on the landscape that accumulated prior to the most recent period of exposure. In cases where subglacial erosion is less than 3 m, measured ^{10}Be concentrations reflect ^{10}Be accumulated from not only the most recent period of surface exposure but also a previous period(s) of surface exposure (i.e., isotopic inheritance). Using the original author's interpretations, our compilation of ^{10}Be ages reveals that isotopic inheritance is minimal along western and southwestern Greenland (14% of measurements), whereas significantly more isotopic inheritance is found in eastern and northern Greenland (41%) and Baffin Island (31%; Figure 4; see Data Repository in Tables S3 and S4). On Baffin Island, extensive work has demonstrated the widespread occurrence of isotopic inheritance in a variety of settings [*Briner et al*., 2006, 2008], yet directly across Baffin Bay at the same latitude in the Sermeq Kujalleq region, the landscape is almost inheritance free [*Corbett et al*., 2011; *Young et al*., 2013b; *Kelley et al*., 2013; *Carlson et al*., 2014]. The most obvious exception to this general pattern of minimal inheritance in western and southwestern Greenland is inherited ^{10}Be at high elevations where ice was likely thin and cold based during the last glacial cycle [e.g., *Corbett et al*., 2013; *Larsen et al*., 2014]. In a similar fashion, in landscapes dominated by cold based or polythermal ice along Baffin Island and eastern Greenland, isotopic inheritance is minimal in zones of selective linear erosion [e.g., *Briner et al*., 2009; *Young et al*., 2012; *Hughes et al*., 2012; *Dyke et al*., 2014]. Although local factors can influence the magnitude of subglacial erosion and no single region is completely immune to isotopic inheritance, the limited number of erosion estimates coupled with the spatial distribution of isotopic inheritance in the Baffin Bay-Greenland region suggests that regional climate gradients influence subglacial thermal regimes and long-term erosion rates.

5. Conclusions

High-precision ^{10}Be measurements coupled with historical observations and detailed geological reconstructions of ice-margin change allow direct quantification of a subglacial abrasion rate beneath the western GrIS of 0.72 ± 0.35 mm yr^{-1} and an inferred total basin-wide erosion rate of ~1–1.8 mm yr^{-1}. Regardless of which estimate of total subglacial erosion is used from western Greenland (this study versus sediment-based studies), subglacial erosion beneath the western GrIS is at least 1 order of magnitude greater than previously published polar glacial erosion rates. Assuming a constant erosion rate of 1.0–1.8 mm yr^{-1} from southwestern Greenland, only ~1670–3000 years of ice cover during the last glacial cycle is needed to erode through the ~3 m of rock required to reset the cosmogenic clock. Much slower or variable rates of erosion would also likely be sufficient to reset the cosmogenic clock as the landscape in southwestern Greenland experienced several tens of thousands of years of ice cover during the last glacial cycle. Indeed, erosion was almost certainly slower and spatially variable during the last glacial cycle because a constant erosion rate of 1.0–1.8 mm yr^{-1} would result in an unlikely several tens to hundreds of meters of bedrock removal. Nonetheless, high subglacial erosion rates in western Greenland over historical times likely explain the relative lack of isotopic inheritance in published ^{10}Be data sets from the region when projected through

the last glacial cycle. The western GrIS's elevated subglacial erosion rates are at least in part dictated by the relatively mild climate along western Greenland, which encourages warm based and erosive ice; the more common presence of isotopic inheritance from Arctic northern and eastern Greenland and Baffin Island is indicative of lower long-term subglacial erosion rates dictated by cold based to polythermal ice. Finally, in situ ^{10}Be measurements from eroded bedrock offer a powerful approach to quantify subglacial erosion rates in settings where the glacial-geologic history is well constrained and also offers an opportunity to further quantify the relative contributions of abrasion and quarrying to the overall subglacial erosion budget.

Appendix A

The following studies from the Baffin-Bay-Greenland region are included in our ^{10}Be age compilation.

Baffin Island *Bierman et al.* [1999a, 1999b], *Bierman et al.* [2001], *Briner et al.* [2003], *Briner et al.* [2005], *Briner et al.* [2006], *Briner et al.* [2007], *Briner et al.* [2009], *Briner et al.* [2013a], *Corbett et al.* [2016], *Davis et al.* [1999], *Davis et al.* [2006], *Kaplan et al.* [2001], *Kaplan and Miller* [2003], *Margreth et al.* [2016], *Marsella* [1998], *Marsella et al.* [2000], *McCuaig* [1994], *Miller et al.* [2005], *Miller et al.* [2006], *Steig et al.* [1998], *Utting et al.* [2007], *Young et al.* [2012], and *Young et al.* [2015].

Greenland *Alexanderson and Håkansson* [2014], *Briner et al.* [2013b], *Carlson et al.* [2014], *Corbett et al.* [2011], *Corbett et al.* [2013], *Corbett et al.* [2015], *Cronauer et al.* [2016], *Dyke et al.* [2014], *Håkansson et al.* [2007a], *Håkansson et al.* [2007b], *Håkansson et al.* [2009], *Håkansson et al.* [2011], *Hughes et al.* [2012], *Kelley et al.* [2013], *Kelley et al.* [2015], *Kelly et al.* [2008], *Lane et al.* [2014], *Larsen et al.* [2014], *Larsen et al.* [2016], *Levy et al.* [2012], *Levy et al.* [2013], *Levy et al.* [2016], *Lowell et al.* [2013], *Möller et al.* [2010], *Nelson et al.* [2014], *Rinterknecht et al.* [2009], *Rinterknecht et al.* [2014], *Roberts et al.* [2008], *Roberts et al.* [2009], *Roberts et al.* [2013], *Winsor et al.* [2014], *Winsor et al.* [2015], *Young et al.* [2011], *Young et al.* [2013a], and *Young et al.* [2013b].

Acknowledgments

N. Young and J. Schaefer acknowledge partial support from the Comer Science and Educational Foundation. N. Young also received generous support from a Lamont-Doherty Postdoctoral Fellowship and Research Professorship. We thank R. Schwartz, J. Hanley, and J. Frisch for help with ^{10}Be sample processing, and we thank S. Zimmerman and R. Finkel for careful ^{10}Be measurements at Lawrence Livermore National Laboratory's Center for Accelerator Mass Spectrometry. The raw data can be found in the accompanying supporting information or by contacting the corresponding author (N. Young). The authors declare no competing financial interests. We thank J. Heyman and an anonymous reviewer for their helpful reviews. This is LDEO contribution 8069.

References

Alexanderson, H., and L. Håkansson (2014), Coastal glaciers advanced onto Jameson Land, East Greenland during the late glacial-early Holocene Milne Lane Stade, *Polar Res.*, *33*, 20,313.

Andrews, J. T., J. D. Milliman, A. E. Jennings, N. Rynes, and J. Dwyer (1994), Sediment thickness and Holocene glacial marine sedimentation rates in three east Greenland fjords (ca. 68°N), *J. Geol.*, *102*, 669–683.

Applegate, P. J., N. Kirchner, E. J. Stone, K. Keller, and R. Greve (2012), An assessment of key model parametric uncertainties in projections of Greenland Ice Sheet behavior, *Cryosphere*, *6*, 589–606, doi:10.5194/tc-6-589-2012.

Balco, G., J. O. Stone, N. A. Lifton, and T. J. Dunai (2008), A complete and easily accessible means of calculating surface exposure ages and erosion rates from ^{10}Be and ^{26}Al measurements, *Quat. Geochron.*, *3*, 174–195.

Bierman, P. R., K. A. Marsella, C. Patterson, P. T. Davis, and M. Caffee (1999a), Mid-Pleistocene cosmogenic minimum-age limits for pre-Wisconsinan glacial surfaces in southwestern Minnesota and southern Baffin Island: A multiple nuclide approach, *Geomorphology*, *27*, 25–39.

Bierman, P. R., K. A. Marsella, C. Patterson, P. T. Davis, and M. Caffee (1999b), Response to discussion by Wolfe et al, *Geomorphology*, *39*, 255–260.

Bierman, P. R., K. A. Marsella, P. Thompson Davis, and M. W. Caffee (2001), Response to discussion by Wolfe et al. on Bierman et al. (Geomorphology 25 (1999) 25-9), *Geomorphology*, *39*, 255–260.

Boulton, G. S. (1979), Processes of glacier erosion on different substrates, *J. Glaciol.*, *23*, 15–38.

Briner, J. P., and T. W. Swanson (1998), Using inherited cosmogenic Cl-36 to constrain glacial erosion rates of the Cordilleran ice sheet, *Geology*, *26*, 3–6.

Briner, J. P., G. H. Miller, P. T. Davis, P. R. Bierman, and M. Caffee (2003), Last Glacial Maximum ice sheet dynamics in Arctic Canada inferred from young erratics perched on ancient tors, *Quat. Sci. Rev.*, *22*, 437–444.

Briner, J. P., G. H. Miller, P. T. Davis, and R. C. Finkel (2005), Cosmogenic exposure dating in arctic glacial landscapes: Implications for the glacial history of northeastern Baffin Island, Arctic Canada, *Can. J. Earth. Sci.*, *42*, 67–84.

Briner, J. P., G. H. Miller, P. T. Davis, and R. C. Finkel (2006), Cosmogenic radionuclides from fiord landscapes support differential erosion by overriding ice sheets, *Geol. Soc. Am. Bull.*, *118*, 406–420, doi:10.1130/B25716.1.

Briner, J. P., I. Overeem, G. Miller, and R. Finkel (2007), The deglaciation of Clyde Inlet, northeastern Baffin Island, Arctic Canada, *J. Quat. Sci.*, *22*, 223–232.

Briner, J. P., G. H. Miller, R. Finkel, and D. P. Hess (2008), Glacial erosion at the fjord onset zone and implications for the organization of ice flow on Baffin Island, Arctic Canada, *Geomorphology*, *97*, 126–134, doi:10.1016/j.geomorph.2007.02.039.

Briner, J. P., A. C. Bini, and R. S. Anderson (2009), Rapid early Holocene retreat of a Laurentide outlet glacier through an Arctic fjord, *Nat. Geosci.*, *2*, 496–499, doi:10.1038/ngeo556.

Briner, J. P., H. A. M. Stewart, N. E. Young, W. Philipps, and S. Losee (2010), Using proglacial-threshold lakes to constrain fluctuations of the Jakobshavn Isbræ ice margin, western Greenland, during the Holocene, *Quat. Sci. Rev.*, *29*, 3861–3874, doi:10.1016/j.quascirev.2010.09.005.

Briner, J. P., N. E. Young, E. K. Thomas, H. A. M. Stewart, S. Losee, and S. Truex (2011), Varve and radiocarbon dating support the rapid advance of Jakobshavn Isbræ during the Little Ice Age, *Quat. Sci. Rev.*, *30*, 2476–2486, doi:10.1016/j.quascirev.2011.05.017.

Briner, J. P., N. A. Lifton, G. H. Miller, K. Refsnider, R. Anderson, and R. Finkel (2013a), Using in situ cosmogenic ^{10}Be, ^{14}C, and ^{26}Al to decipher the history of polythermal ice sheets on Baffin Island, Arctic Canada, *Quat. Geochron.*, *19*, 4–13.

Briner, J. P., L. Häkansson, and O. Bennike (2013b), The deglaciation and neoglaciation of Upernavik Isstrøm, Greenland, *Quat. Res.*, *80*, 459–467.

Carlson, A. E., K. Winsor, D. J. Ullman, E. J. Brook, D. H. Rood, Y. Axford, A. N. LeGrande, F. S. Anslow, and G. Sinclair (2014), Earliest Holocene south Greenland ice sheet retreat within its late Holocene extent, *Geophys. Res. Lett.*, *41*, 5514–5521, doi:10.1002/2014GL060800.

Cohen, D., N. R. Iverson, T. S. Hooyer, U. H. Fischer, M. Jackson, and P. L. Moore (2005), Debris-bed friction of hard-bedded glaciers, *J. Geophys. Res.*, *110*, F02007, doi:10.1029/2004JF000228.

Corbett, L. B., N. E. Young, P. R. Bierman, J. P. Briner, T. A. Neumann, D. H. Rood, and J. A. Graly (2011), Paired bedrock and boulder ^{10}Be concentrations resulting from early Holocene ice retreat near Jakobshavn Isfjord, western Greenland, *Quat. Sci. Rev.*, *30*, 1739–1749, doi:10.1016/j.quascirev.2011.04.001.

Corbett, L. B., P. R. Bierman, J. A. Graly, T. A. Neumann, and D. H. Rood (2013), Constraining landscape history and glacial erosivity using paired cosmogenic nuclides in Upernavik, northwest Greenland, *Geol. Soc. Am. Bull.*, *125*, 1539–1553, doi:10.1130/B30813.1.

Corbett, L. B., P. R. Bierman, G. Everett Lasher, and D. H. Rood (2015), Landscape chronology and glacial history in Thule, northwest Greenland, *Quat. Sci. Rev.*, *109*, 57–67.

Corbett, L. B., P. Bierman, and P. Thompson Davis (2016), Glacial history and landscape evolution of southern Cumberland Peninsula, Baffin Island, Canada, constrained by cosmogenic ^{10}Be and ^{26}Al, *Earth Planet. Sci. Lett.*, *128*, 1173–1192.

Cowton, T., P. Nienow, I. Bartholomew, A. Sole, and D. Mair (2012), Rapid erosion beneath the Greenland ice sheet, *Geology*, *40*, 343–346, doi:10.1130/G32687.1.

Cronauer, S. L., J. P. Briner, S. E. Kelley, S. R. H. Zimmerman, and M. Morlighem (2016), ^{10}Be dating reveals early-middle Holocene age of the Drygalski Moraines in central West Greenland, *Quat. Sci. Rev.*, *147*, 59–68.

Csatho, B., T. Schenk, C. J. van der Veen, and W. B. Krabill (2008), Intermittent thinning of Jakobshavn Isbrae, West Greenland, since the little ice age, *J. Glaciol.*, *54*, 131–144.

Davis, P. T., P. R. Bierman, K. A. Marsella, M. W. Caffee, and J. R. Southon (1999), Cosmogenic analysis of glacial terrains in the eastern Canadian Arctic: A test for inherited nuclides and the effectiveness of glacial erosion, *Ann. Glaciol.*, *28*.

Davis, P. T., J. P. Briner, R. D. Coulthard, R. C. Finkel, and G. H. Miller (2006), Preservation of Arctic landscapes overridden by cold-based ice sheets, *Quat. Res.*, *65*, 156–163.

Duhnforth, M., R. S. Anderson, D. Ward, and G. M. Stock (2010), Bedrock fracture control of glacial erosion processes and rates, *Geology*, *38*, 423–426, doi:10.1130/G30576.1.

Dyke, L. M., A. L. C. Hughes, T. Murray, J. F. Hiemstra, C. S. Andresen, and Á. Rodés (2014), *Quat. Sci. Rev.*, *99*, 244–259, doi:10.1016/j.quascirev.2014.06.001.

Garde, A. A., and A. Steenfelt (1999), Precambrian geology of Nuussuaq and the area north-east of Disko Island, In Precambrian geology of the Disko Bugt region, west Greenland, in *Geology of Greenland Survey Bulletin*, vol. 181, edited by F. Kalsbeek, 6 pp., Copenhagen.

Goehring, B. M., J. M. Schaefer, C. Schluechter, N. A. Lifton, R. C. Finkel, A. J. T. Jull, N. Akçar, and R. B. Alley (2011), The Rhone Glacier was smaller than today for most of the Holocene, *Geology*, *39*, 679–682, doi:10.1130/G32145.1.

Greve, R., F. Saito, and A. Abe-Ouchi (2011), Initial results of the SeaRISE numerical experiments with the models SICOPOLIS and IcIES for the Greenland Ice Sheet, *Ann. Glaciol.*, *52*, 23–30.

Gurnell, A. (1987), Fluvial sediment yield from Alpine, glacierized catchments, in *Glacio-Fluvial Sediment Transfer An Alpine Perspective*, edited by A. Gurnell and M. Clark, pp. 415–420 , John Wiley & Sons, New York.

Hallet, B., L. Hunter, and J. Bogen (1996), Rates of erosion and sediment evacuation by glaciers: A review of field data and their implications, *Global Planet. Change*, *12*, 213–235.

Håkansson, L., J. Briner, H. Alexanderson, A. Aldahan, and G. Possnert (2007a), ^{10}Be ages from central east Greenland constrain the extent of the Greenland ice sheet during the Last Glacial Maximum, *Quat. Sci. Rev.*, *26*, 2316–2321.

Håkansson, L., A. Graf, S. Strasky, S. Ivy-Ochs, P. W. Kubik, C. Hjort, and C. Schlüchter (2007b), Cosmogenic ^{10}Be-ages from the Store Koldewey Island, NE Greenland, *Geogr. Ann. A.*, *89A*, 195–202.

Håkansson, L., H. Alexanderson, C. Hjort, P. Möller, J. P. Briner, A. Aldahan, and G. Possnert (2009), Late Pleistocene glacial history of Jameson Land, central east Greenland, derived from cosmogenic ^{10}Be and ^{26}Al exposure dating, *Boreas*, *38*, 244–260.

Håkansson, L., J. Briner, A. Aldahan, and G. Possnert (2011), ^{10}Be data from meltwater channels suggest that Jameson Land, east Greenland, was ice-covered during the last glacial maximum, *Quat. Res.*, *76*, 452–459.

Harbor, J. M., B. Hallet, and C. F. Raymond (1988), A numerical model of land-form development by glacial erosion, *Nature*, *333*, 347–349.

Heisinger, B., D. Lal, A. Jull, P. Kubik, S. Ivy-Ochs, K. Knie, and E. Nolte (2002a), Production of selected cosmogenic radionuclides by muons: 2. Capture of negative muons, *Earth. Planet. Sc. Lett.*, *200*, 357–369.

Heisinger, B., D. Lal, A. Jull, P. Kubik, S. Ivy-Ochs, S. Neumaier, K. Knie, V. Lazarev, and E. Nolte (2002b), Production of selected cosmogenic radionuclides by muons 1. Fast muons, *Earth Planet. Sci. Lett.*, *200*, 345–355.

Herman, F., O. Beyssac, M. Brughelli, S. N. Lane, S. Leprince, T. Adatte, J. Y. Y. Lin, J.-P. Avouac, and S. C. Cox (2015), Erosion by an Alpine glacier, *Science*, *350*, 193–195, doi:10.1126/science.aab2386.

Hughes, A. L. C., E. Rainsley, T. Murray, C. J. Fogwill, C. Schnabel, and S. Xu (2012), Rapid response of Helheim Glacier, southeast Greenland, to early Holocene climate warming, *Geology*, *40*, 427–430, doi:10.1130/G32730.1.

Iverson, N. R., and L. K. Zoet (2015), Experiments on the dynamics and sedimentary products of glacier slip, *Geomorphology*, *244*, 121–134, doi:10.1016/j.geomorph.2015.03.027.

Jaeger, J. M., and M. N. Koppes (2016), The role of the cryosphere in source-to-sink systems, *Earth Sci. Rev.*, *153*, 43–76, doi:10.1016/j.earscirev.2015.09.011.

Joughin, I., B. E. Smith, D. E. Shean, and D. Floricioiu (2014), Brief communication: Further summer speedup of Jakobshavn Isbræ, *Cryosphere*, *8*, 209–214, doi:10.5194/tc-8-209-2014.

Joughin, I., B. E. Smith, I. M. Howat, T. Scambos, and T. Moon (2010), Greenland flow variability from ice-sheet-wide velocity mapping, *J. Glaciol.*, *56*, 415–430.

Kaplan, M. R., G. H. Miller, and E. J. Steig (2001), Low-gradient outlet glaciers (ice streams?) drained the Laurentide ice sheet, *Geology*, *29*, 343–346.

Kaplan, M. R., and G. H. Miller (2003), Early Holocene delevelling and deglaciation of the Cumberland Sound region, Baffin Island, Arctic Canada, *Geol. Soc. Am. Bull.*, *115*, 445–462.
Kelley, S. E., J. P. Briner, and N. E. Young (2013), Rapid ice retreat in Disko Bugt supported by ^{10}Be dating of the last recession of the western Greenland Ice Sheet, *Quat. Sci. Rev.*, *82*, 13–22, doi:10.1016/j.quascirev.2013.09.018.
Kelley, S. E., J. P. Briner, and S. R. H. Zimmerman (2015), The influence of ice marginal setting on early Holocene retreat rates in central West Greenland, *J. Quat Sci.*, *30*, 271–280.
Kelly, M. A., T. V. Lowell, B. L. Hall, J. M. Schaefer, R. C. Finkel, B. M. Goehring, R. B. Alley, and G. H. Denton (2008), A ^{10}Be chronology of late glacial and Holocene mountain glaciation in the Scoresby Sund region, east Greenland: Implications for seasonality during late glacial time, *Quat. Sci. Rev.*, *27*, 2273–2282.
Koppes, M. N., and D. R. Montgomery (2009), The relative efficacy of fluvial and glacial erosion over modern to orogenic timescales, *Nat. Geosci.*, *2*, 644–647, doi:10.1038/ngoe616.
Koppes, M., B. Hallet, E. Rignot, J. Mouginot, J. S. Wellner, and K. Boldt (2015), Observed latitudinal variations in erosion as a function of glacier dynamics, *Nature*, *526*, 100–103, doi:10.1038/nature15385.
Koppes, M., R. Sylwester, A. Rivera, and B. Hallet (2010), Variations in sediment yield over the advance and retreat of a calving glacier, Laguna San Rafael, North Patagonian Icefield, *Quat. Res.*, *73*, 84–95, doi:10.1016/j.yqres.2009.07.006.
Lal, D. (1991), Cosmic-ray labeling of erosion surfaces—In situ nuclide production-rates and erosion models, *Earth. Planet. Sc. Lett.*, *104*, 424–439.
Lane, T. P., D. H. Roberts, B. R. Rea, C. Ó. Cofaigh, A. Vieli, and A. Rodés (2014), Controls upon the Last Glacial Maximum deglaciation of the northern Uummannaq Ice Stream System, West Greenland, *Quat. Sci. Rev.*, *92*, 324–344.
Larsen, N. K., S. Funder, K. H. Kjær, and K. K. Kjeldsen (2014), Rapid early Holocene ice retreat in West Greenland, *Quat. Sci. Rev.*, doi:10.1016/j.quascirev.2013.05.027.
Larsen, N. K., S. Funder, H. Linge, P. Möller, A. Schomaker, D. Fabel, S. Xu, and K. Kjær (2016), A Younger Dryas re-advance of local glaciers in north Greenland, *Quat. Sci. Rev.*, *147*, 47–58.
Lecavalier, B., et al. (2014), A model of Greenland ice sheet deglaciation constrained by observations of relative sea level, *Quat. Sci. Rev.*, *102*, 54–84.
Levy, L., M. A. Kelly, J. A. Howley, and R. A. Virginia (2012), Age of the Orkendalen moraines, Kangerlussuaq, Greenland: Constraints on the extent of the southwestern margin of the Greenland Ice Sheet during the Holocene, *Quat. Sci. Rev.*, *52*, 1–5.
Levy, L. B., M. A. Kelly, T. V. Lowell, B. L. Hall, L. A. Hempel, W. M. Honsaker, A. R. Lusas, J. A. Howley, and Y. L. Axford (2013), Holocene fluctuations of Bregne ice cap, Scoresby Sund, east Greenland: A proxy for climate along the Greenland Ice Sheet margin, *Quat. Sci. Rev.*, *92*, 357–368.
Levy, L. B., M. A. Kelly, T. A. Lowell, B. L. Hall, J. A. Howley, and C. A. Smith (2016), Coeval fluctuations of the Greenland ice sheet and a local glacier, central East Greenland, during late glacial and early Holocene time, *Geophys. Res. Lett.*, *43*, 1623–1631, doi:10.1002/2015GL067108.
Lowell, T. V., B. L. Hall, M. A. Kelly, O. Bennike, A. R. Lusas, W. Honsaker, C. A. Smith, L. B. Levy, S. Travis, and G. H. Denton (2013), Late Holocene expansion of Istorvet ice cap, Liverpool Land, east Greenland, *Quat. Sci. Rev.*, *63*, 128–140.
Margreth, A., J. C. Gosse, and A. S. Dyke (2016), Quantification of subaerial and episodic subglacial erosion rates on high latitude upland plateaus: Cumberland Peninsula, Baffin Island, Arctic Canada, *Quat. Sci. Rev.*, *133*, 108–129.
Marsella, K. A. (1998), Timing and extent of glaciation in the Pangnirtung Fjord Region, Baffin Island: Determined using in situ produced cosmogenic ^{10}Be and ^{26}Al. *Master of Science Dissertation*, University of Vermont, Burlington, Vt.
Marsella, K. A., P. Bierman, P. T. Davis, and M. W. Caffe (2000), Cosmogenic 10Be and 26Al ages for the Last Glacial Maximum, eastern Baffin Island, Arctic Canada, *Geol. Soc. Am. Bull.*, *112*, 1296–1312.
McCuaig, S. J. (1994), Glacial chronology of the south Bylot and Salmon River lowlands, N.W.T., using erratic dispersal patterns, cosmogenic dating, radiocarbon dating and lichenometry, MS thesis, Carleton Univ., Ottawa.
Miller, G. H., A. P. Wolfe, J. P. Briner, P. J. Sauer, and A. Nesje (2005), Holocene glaciation and clime evolution of Baffin Island, Arctic Canada, *Quat. Sci. Rev.*, *24*, 1703–1721.
Miller, G. H., J. P. Briner, N. A. Lifton, and R. C. Finkel (2006), Limited ice-sheet erosion and complex histories derived from in situ cosmogenic ^{10}Be, ^{26}Al, and ^{14}C on Baffin Island, Arctic Canada, *Quat. Geochron.*, *1*, 74–85.
Möller, P., N. K. Larsen, K. H. Kjær, S. Funder, A. Schomacker, H. Linge, and D. Fabel (2010), Early to middle Holocene valley glaciations on northernmost Greenland, *Quat. Sci. Rev.*, *29*, 3379–3398.
Nelson, A. H., P. R. Bierman, J. D. Shakun, and D. H. Rood (2014), Using *in situ* cosmogenic ^{10}Be to identify the source of sediment leaving Greenland, *Earth. Surf. Processes.*, *39*(1), 1087–1100.
Nishiizumi, K., M. Imamura, M. W. Caffee, J. R. Southon, R. C. Finkel, and J. McAninch (2007), Absolute calibration of ^{10}Be AMS standards, *Nucl. Instrum. Meth. B.*, *258*, 403–413.
Rignot, E., and P. Kanagaratnam (2006), Changes in the velocity structure of the Greenland ice sheet, *Science*, *311*, 986–990, doi:10.1126/science.1121381.
Riihimaki, C. A., K. R. MacGregor, R. S. Anderson, S. P. Anderson, and M. G. Loso (2005), Sediment evacuation and glacial erosion rates at a small alpine glacier, *J. Geophys. Res.*, *110*, F03003, doi:10.1029/2004JF000189.
Rinterknecht, V., Y. Gorokhovich, J. Schaefer, and M. Caffee (2009), Preliminary ^{10}Be chronology for the last deglaciation of the western margin of the Greenland Ice Sheet, *J. Quat. Sci.*, *24*, 270–278.
Rinterknecht, V., V. Jomelli, D. Brunstein, V. Favier, V. Masson-Delmotte, D. Bourlès, L. Leanni, and R. Schläppy (2014), Unstable ice stream in Greenland during the Younger Dryas cold event, *Geology*, *42*, 759–762.
Roberts, D. H., A. J. Long, C. Schnabel, S. Freeman, and M. J. R. Simpson (2008), The deglacial history of southeast sector of the Greenland Ice Sheet during the Last Glacial Maximum, *Quat. Sci. Rev.*, *27*, 1505–1516.
Roberts, D. H., A. J. Long, C. Schnabel, B. J. Davies, S. Xu, M. J. R. Simpson, and P. Huybrechts (2009), Ice sheet extent and early deglacial history of the southwestern sector of the Greenland Ice Sheet, *Quat. Sci. Rev.*, *28*, 2760–2773.
Roberts, D. H., B. R. Rea, T. P. Lane, C. Schnabel, and A. Rodés (2013), New constraints on Greenland ice sheet dynamics during the last glacial cycle: Evidence from the Uummannaq ice stream system, *J. Geophys Res. Earth Surf.*, *118*, 519–541.
Schaefer, J. M., et al. (2009), High-frequency Holocene glacier fluctuations in New Zealand differ from the northern signature, *Science*, *324*, 622–625, doi:10.1126/science.1169312.
Steig, E. J., A. P. Wolfe, and G. H. Miller (1998), Wisconsinan refugia and the glacial history of eastern Baffin Island, Arctic Canada: Coupled evidence from cosmogenic isotopes and lake sediments, *Geology*, *26*, 835–838.
Stone, J. O. (2000), Air pressure and cosmogenic isotope production, *J. Geophys. Res.*, *105*, 753–23,759.
Stroeven, A. P., D. Fabel, C. Hättestrand, and J. Harbor (2002), A relict landscape in the centre of Fennoscandian glaciation: Cosmogenic radionuclide evidence of tors preserved through multiple glacial cycles, *Geomorphology*, *44*(1–2), 145–154.

Ugelvig, S. V., D. L. Egholm, and N. R. Iverson (2016), Glacial landscape evolution by subglacial quarrying: A multi-scale computational approach, *J. Geophys. Res. Earth Surface*, doi:10.1002/2016JF003960.

Utting, D. J., J. C. Gosse, D. A. Hodgson, M. S. Trommelen, K. J. Vickers, S. E. Kelley, and B. Ward (2007), Report on ice-flow history, deglacial chronology, and surficial geology, Foxe Peninsula, southwest Baffin Island, Nunavut, *Geol. Surv. Can., Curr. Res.*, 2007-C2, 13 pp.

Weidick, A. (1968), Observations on some Holocene glacier fluctuations in west Greenland, *Meddelelsser om Grønland, 165*, 202 pp.

Weidick, A., and O. Bennike (2007), Quaternary glaciation history and glaciology of Jakobshavn Isbrae and the Disko Bugt region, West Greenland: A review, in *Geological Survey of Denmark and Greenland Bulletin*, vol. 14.

Wimpenny, J., R. H. James, K. W. Burton, A. Gannoun, F. Mokadem, and S. R. Gíslason (2010), Glacial effects on weathering processes: New insights from the elemental and lithium isotopic composition of West Greenland rivers, *Earth. Planet. Sc. Lett.*, *290*, 427–437, doi:10.1016/j.epsl.2009.12.042.

Winsor, K., A. E. Carlson, and D. H. Rood (2014), ^{10}Be dating of the Narsarsuaq moraine in southernmost Greenland: Evidence for a late-Holocene ice advance exceeding the Little Ice Age maximum, *Quat. Sci. Rev.*, *98*, 135–143.

Winsor, K., A. E. Carlson, M. W. Caffee, and D. H. Rood (2015), Rapid last-deglacial thinning and retreat of the marine-terminating southwestern Greenland ice sheet, *Earth Planet. Sci. Lett.*, *426*, 1–12.

Young, N. E., J. P. Briner, H. A. M. Stewart, Y. Axford, B. Csatho, D. H. Rood, and R. C. Finkel (2011), Response of Jakobshavn Isbræ, Greenland, to Holocene climate change, *Geology*, *39*, 131–134, doi:10.1130/G31399.1.

Young, N. E., J. P. Briner, D. H. Rood, and R. C. Finkel (2012), Glacier extent during the younger Dryas and 8.2-ka event on Baffin Island, Arctic Canada, *Science*, *337*(6100), 1330–1333, doi:10.1126/science.1222759.

Young, N. E., J. M. Schaefer, J. P. Briner, and B. M. Goehring (2013a), A ^{10}Be production-rate calibration for the Arctic, *J. Quat. Sci.*, *28*, 515–526, doi:10.1002/jqs.2642.

Young, N. E., J. P. Briner, D. H. Rood, R. C. Finkel, L. B. Corbett, and P. R. Bierman (2013b), Age of the Fjord Stade moraines in the Disko Bugt region, western Greenland, and the 9.3 and 8.2 ka cooling events, *Quat. Sci. Rev.*, *60*, 76–90, doi:10.1016/j.quascirev.2012.09.028.

Young, N. E., A. D. Schweinsberg, J. P. Briner, and J. M. Schaefer (2015), Glacier maxima in Baffin Bay during the Medieval Warm Period coeval with Norse settlement, *Sci. Adv.*, *1*, e1500806.